Original article

An optical model and experimental analysis of a reflective diffraction grating

Chuang M.H

Submitted: July 12, 2024, Revised: version 1, January 29, 2025, version 2, February 2, 2025, version 3, February 22, 2025
Accepted: February 24, 2025

Abstract
This study examined the optical properties of diffraction patterns produced when a filament lamp illuminated the back of an optical disc. A comprehensive model was constructed that described the wavelength, intensity, and spatial distribution of diffraction lines, considering factors such as disc tilt, track pitch, cross-track interference, and the relative positions of the light source and observer. Experimental validation was performed using CDs, DVDs, and BDs with a precisely controlled setup. Prism dispersion and laser calibration techniques analyzed composite light, with results closely matching theoretical predictions. Key findings included the correlation between tilting angle and wavelength, the confirmation of cross-track interference, the effects of disc recording, and the non-linear line bending at close light-source distances. Additionally, the study explored wavelength distribution across the disc and curved diffraction line formation. These findings enhance the understanding of reflective diffraction gratings and everyday optical phenomena.

Keywords
Physics, Optics, Diffraction grating, Prism, Wavelength superposition, Pitch, Recorded disc, Laser calibration, Cross-track interference, DVD

Min-Hsiang Chuang, Concordia Middle and High School, No. 31 號, Section 2, Jianguo Rd, Minxiong Township, Chiayi County, Taiwan 621 s1110279@my.cmsh.cyc.edu.tw

Introduction

Optical devices, which rely on the principles of light refraction and reflection, are ubiquitous in daily life. When an optical disc is used as a diffraction grating and illuminated by a light source, a distinctive diffraction line appears along its diameter, as shown in Figure 1. The disc's periodic structure consists of closely spaced concentric tracks that function as slits, with their pitch determining the diffraction pattern. Since the back of the CD has a periodic structure, light scattered from different tracks produces interference. Constructive interference takes place when the light path difference is an integral multiple of the wavelength. Constructive and destructive interference patterns can be observed at various angles due to the circular arrangement of the tracks. The grating equation defines the relationship between the diffraction angle, light wavelength, and pitch, which; in turn, determines the observed diffraction pattern.

The optical disc thus acts as a simple STEM tool and a reflective diffraction grating. The disc structure, including the multilayers of a CD, DVD and BD are shown in reference (1). The diffraction patterns from these recording media can be demonstrated in classrooms to introduce diffraction grating concepts (2-6).

Fernandez-Dorado et al. introduced a quantitative method in their study, 'A Simple Experiment to Distinguish Between Replicated and Duplicated Compact Discs Using Fraunhofer Diffraction' (7). Their research demonstrated that subtle differences in the microstructures of the CDs led to distinct diffraction patterns when laser light struck the surface at nearly normal incidence. Furthermore, the study explored the influence of different layers of the disc using the Fraunhofer diffraction model (8). The Fraunhofer diffraction model used Fourier transforms to calculate the resulting pattern at a large distance from the diffracting object.

The study by Fowles, "A Compact Disc Under Skimming Light Rays" (9), investigated the diffraction effects of CDs when illuminated by skimming light rays. The paper explained the formation of colored lines, such as a green line observed when tilted at small angles. However, existing discussions have been limited to small tilt angles and have assumed that the lines are aligned with the center-line of the CD, the observation point, and the source. Therefore, this study includes a discussion of lines in arbitrary spatial positions under general conditions, leading to the discovery of curved lines, as shown in Equations (eq24–eq27) and explained in Experiment 5.

This study investigates the optical properties of the line, as shown in Figure 1, produced when a filament lamp illuminates the back of an optical disc. The investigation analyzes light wavelength and intensity using the characteristics of a reflective diffraction grating (10). Wavelength distribution, and multiple-order superposition are also examined, and mathematical equations are developed describing the line geometry. The theoretical predictions of the proposed optical model were validated by quantitative experimental measurements.

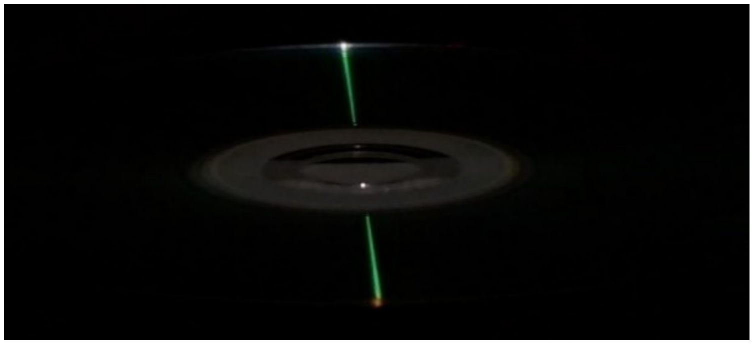

Figure 1. Diffraction pattern observed on an optical disc illuminated by a light source, showing a characteristic green line along the diameter.

Materials and Methods

The apparatus is shown in Figure 2. The experimental setup utilized a 100-watt filament light bulb as the sole light source. A dark environment was created using black clothes to block external light sources and reflections. The disc was positioned 1.5 meters away from the filament light bulb. An Arduino board and motor were employed to control the rotation and precisely adjust the tilting angle of the disc. The setup included a 3D-printed disc holder to ensure stability and precise positioning. This holder facilitated precise tilting increments.

Additionally, laser calibration and cross-track interference verification were performed to analyze specific wavelengths. The laser was employed to verify the phenomenon at predetermined wavelengths. Among these, the results obtained from the laser calibration method were used to analyze wavelengths in subsequent experiments.

The experiment was performed by adjusting the tilting angle of the disc. Using a remote control, the disc was tilted in two-degree intervals, allowing for fine control over the angle of incident light. A Sony Nex-6 camera, with 16.1 MP and 4912 x 3264 resolution, was positioned 1.5m away from the disc to capture the diffraction patterns. The data collected in the experiments ranged from 0 to 90 degrees, at two-degree intervals. The relative intensity was analyzed using grayscale values via ImageJ 1.54d (National Institutes of Health, Bethesda, MD, USA). The absolute intensity was measured using an Ocean Optics USB2000+RAD spectroradiometer (Ocean Optics, Halma PLC, Amersham, UK) and expressed in arbitrary units (a.u.), corresponding to the filament lamp spectrum in Appendix A. This comprehensive setup ensured precise control and detailed analysis of the diffraction patterns.

Three types of optical discs were tested: CDs (1600 nm pitch), DVDs (740 nm pitch), and BDs (320 nm pitch). A prism was installed in front of the camera to disperse non-monochromatic light, as shown in Figure 3. The arrangement of the apparatus is depicted in Figure 4, providing a simplified yet sufficient model for derivation. Additionally, a CD burner was used to record files onto the disc, so as to enable investigation of the effects of recording on the disc.

(a) (b)

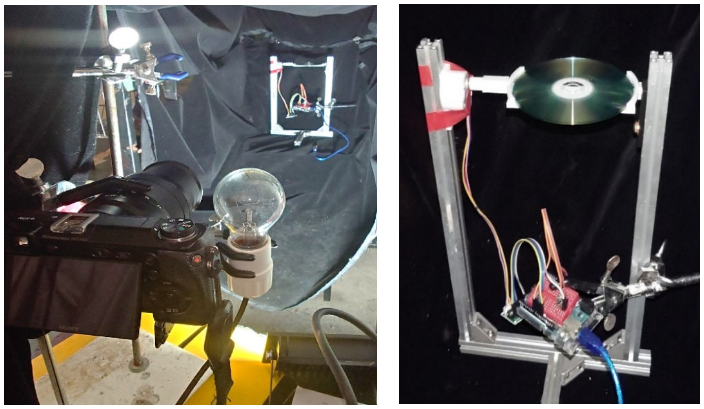

Figure 2. Experiment apparatus. (a) A photo of the experimental apparatus taken in the darkroom. (b) Close-up view of the holder. The CD holder allows the CD to be rotated at different tilting angles.

(a) (b)

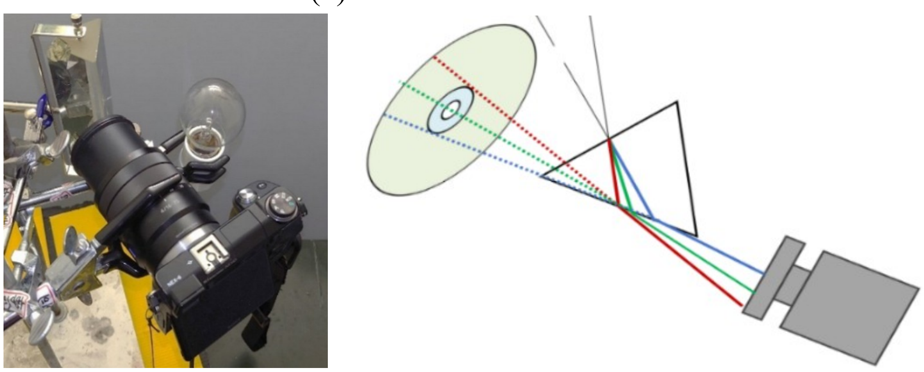

Figure 3. Utilization of prism in the experiment apparatus. (a) Picture of the relative position of the camera, prism, and filament lamp in the experiments. (b) Demonstration of how prism separates the reflected light into various monochromatic lights.

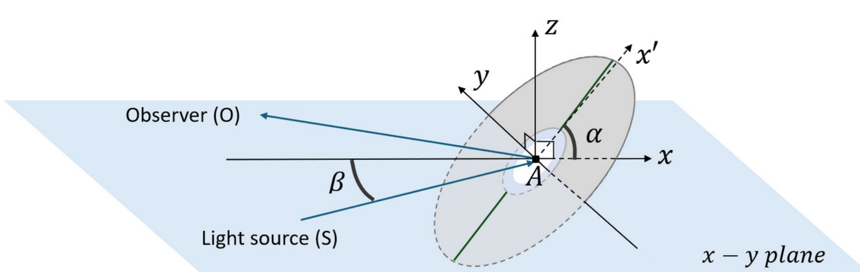

Figure 4. Diagram of the arrangement of experimental apparatus and definition of the coordinate system.

Laser calibration method

This calibration method employed a laser rather than the filament lamp to determine the reflecting position of specific wavelengths. The experimental implementation analyzed the wavelengths of light at different positions by utilizing the principle that different wavelengths refract to distinct positions after passing through a prism. A laser of a specific wavelength was directed at the CD, and the resulting laser spot's coordinates were analyzed to determine the corresponding wavelength. The application of the Cauchy equation (eq1) yielded a fitting function (eq2), which was fitted to the second order with $R^2 > 0.99$, as illustrated in Figure 5. Following calibration, this established relationship enabled the analysis of experiments involving a filament lamp with its continuous spectrum.

$$Cauchy\ equation: n(\lambda) = A + \frac{B}{\lambda^2} + \frac{C}{\lambda^4} + \frac{D}{\lambda^6} + \cdots \quad (1)$$

$$y = 1770 + \frac{1.83 \times 10^8}{\lambda^2} \quad (2)$$

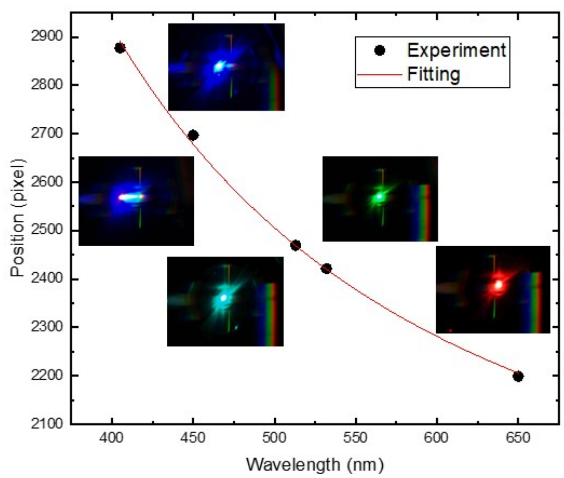

Figure 5. Fitting using Cauchy's equation (1) and photos for each data point using lasers on different wavelengths. The black dots represent experimental data, where the red curve is the fitting line. With a longer wavelength, the included angle from the prism will be bigger, making it on the right side. Vice versa for shorter wavelengths.

All experimental figures were captured at 4912×3264 pixels with the disc fixed in the same position, allowing the line's position to be correlated to the wavelength via equation (eq2). The constants 1770 and 1.83×10^8 originate from the fitted second order curve in Figure 5.

According to Snell's law, the relationship between refractive index and position is nonlinear. However, for small incidence angles, the sine function approximates a linear relationship. Therefore, the Cauchy equation (eq1) was employed to establish the relationship between wavelength and position.

Results and Discussion

Wavelength model

In deriving the wavelength, the optical path difference between light waves diffracted from adjacent tracks was considered. According to diffraction theory, light diffracts based on the spacing between tracks when it encounters the grating. Constructive interference occurs at specific wavelengths that are integer multiples of the grating period, leading to the observed diffraction orders responsible for color formation.

When the disc is tilted, the effective track spacing in the horizontal view changes, resulting in a shift in the perceived colors. This phenomenon is demonstrated in the experiment, where the observed color transitioned from green to blue as the disc was tilted. From a side view of the tilted disc, the spacing between two adjacent tracks is scaled by the cosine of the tilting angle. In the top view, the rotational angle β, defined as the angle between the observer and the normal to the surface, is considered. This variation in track spacing leads to Equation (eq3), which describes the diffraction wavelength. The optical path difference is expressed from both the horizontal and top perspectives, as illustrated in Figures 6(b) and 6(c).

$$\Delta L = m\lambda_m = 2a\cos\alpha\cos\beta \tag{3}$$

Where m is the diffraction order, and a is the pitch. The angles α and β represent the tilting and rotating angles, respectively. The tilting angle α is defined as the angle between the surface of the disc and the xy-plane, as shown in Figures 6(a) and 6(b). The rotating angle β refers to the observer's rotation, depicted in Figure 6(a). Although β remains unchanged in most experiments, it is considered to account for the included angle between the observer, the CD, and the light source. Ultimately, the wavelength can be determined by solving Equation (eq4).

$$\lambda_m = \frac{2a\cos\alpha\cos\beta}{m} \tag{4}$$

Taking a=1600 nm, α=20° and β=0° as an example, wavelengths of the first, second and third orders are thus calculated to be 3007 nm, 1504 nm, and 1002 nm respectively. The fifth to the seventh order wavelengths fall in the visible wavelength range, of 601 nm, 501 nm, and 429 nm, respectively.

Along different positions on the lines, the optical path difference on the CD varies, causing a difference in wavelength. Considering the filament as a point light source, the changes in the angle of incident light cause differences in the wavelength and intensity, as shown in Figure 7.

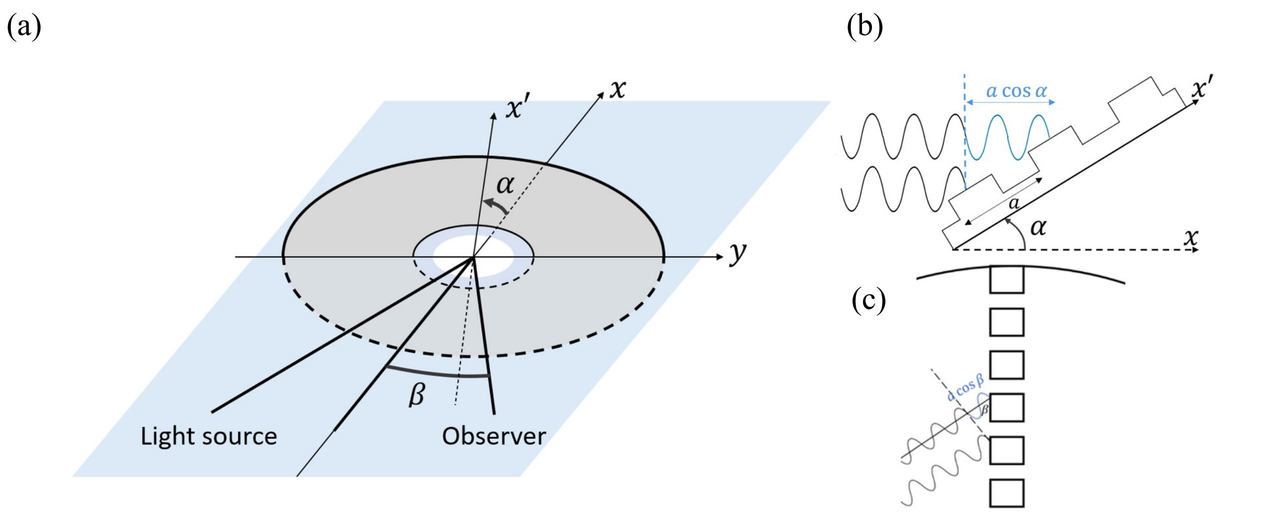

Figure 6. (a) Demonstration of relevant variables and coordination. The disc is tilted with an angle α from the x-y plane, painted in blue, and the disc is located on the x'-y plane. (b) A side view of the optical disc shows the light path difference of interfered light from adjacent tracks, serving as the horizontal component. (c) Top view of the optical disc, showing the light path difference related to the rotating angle β.

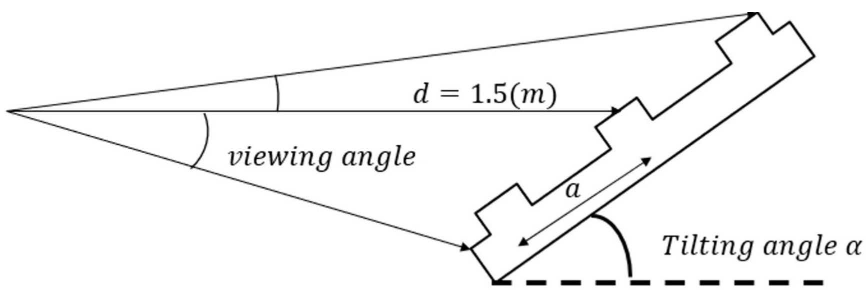

Figure 7. Demonstration of the viewing angle θ.

To account for positional effects, the viewing angle θ is defined as the angle between the horizontal line and the light path to a specific point on the disc.

$$\theta = \tan^{-1}\left(\frac{x' \sin\alpha}{d + x' \cos\alpha}\right), d = 1.5\ (m) \tag{5}$$

Where d is the distance from the disc to the light source and camera, x' refers to the distance to the center of the disc. Thus, the effective tilting angle α' can be written as equations (eq6, eq7). At small values of θ, since the radius of the disc is relatively small, an effective tilting angle relative to the distance to the center of the disc approximates an inverse trigonometric function that is linear within this range.

$$If\ \theta > 0:\ \alpha' = \alpha - \theta \tag{6}$$

$$If\ \theta < 0:\ \alpha' = \alpha + \theta \tag{7}$$

The distance between any point on the CD and its center is relatively small compared to the distance between the center and the light source. As a result, for small portions of the disc, the path can be approximated as a straight line. Once the effective tilting angle α' is determined, it is substituted back into the wavelength equation to compute the corresponding light wavelength, as defined in Equation (eq8).

$$\lambda_m = \frac{2a\cos\alpha'\cos\beta}{m} = \frac{2a\cos(\alpha-\theta)\cos\beta}{m} \tag{8}$$

The current model also considers the light path difference of adjacent tracks. However, the light wave may interfere with tracks crossing a few pits (see next section). Therefore, a constant n needs to be included to represent the number of tracks being crossed by the interfered wave. An example of n=2 is illustrated in Figure 8.

$$\lambda_m = \frac{n \times 2a\cos(\alpha-\theta)\cos\beta}{m} \tag{9}$$

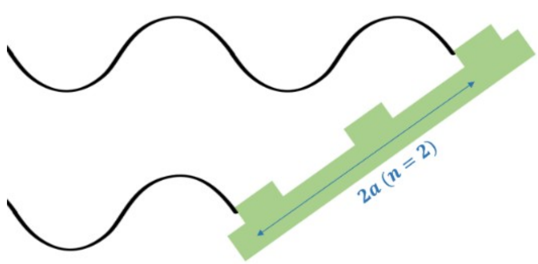

Figure 8. Demonstration of cross-track interference in the case of n=2.

Intensity model

Using the general form of the scalar diffraction theorem, the intensity of light diffracted by the grating lines on the CD surface can be quantified. Considering the x′−y plane and setting the center of the CD as the origin, the variation in optical path length along the x'-axis is analyzed. The total optical path length function h(x') (eq10) is given as

$$Optical\ path\ length: h(x') = 2(d + r_{center} + x' \cos\alpha)\cos\beta \tag{10}$$

Where r_{center} refers to the radius of the central, hollow part of the disc. Assuming the grating has a number N of parallel slits of the same width b and pits distance a, the evaluation of the diffraction integral (eq11) can thus be derived.

$$\int_{Total} e^{ikh(x\prime)} dx' = \left(\int_0^b + \int_a^{a+b} + \int_{2a}^{2a+b} + \dots + \int_{(N-1)a}^{(N-1)a+b}\right) e^{ik\times 2(d+r+x'\cos\alpha)\cos\beta} dx' \tag{11}$$

The sum of the integral is separated into two parts, The first part (eq12, eq13) can be calculated simply since it is a constant integration, given as

$$\int_0^b + \int_a^{a+b} + \int_{2a}^{2a+b} + \dots + \int_{(N-1)a}^{(N-1)a+b} e^{2ik(d+r)\cos\beta} dx' \tag{12}$$

$$[(b-0) + (a+b-a) + \cdots + b] \times e^{2ik(d+r)\cos\beta} = Nbe^{2ik(d+r)\cos\beta} \tag{13}$$

Where N is the total number of tracks on the disc. For the second part (eq14) of the integral, using the identity of the calculation of complex numbers, where k'=kcosαcosβ to reduce the complexity.

$$\int_0^b + \int_a^{a+b} + \int_{2a}^{2a+b} + \dots + \int_{(N-1)a}^{(N-1)a+b} e^{2ikx\prime\cos\alpha\cos\beta} dx' \tag{14}$$

$$\frac{e^{ibk'} - 1}{k'}\left[1 + e^{2iak'} + e^{2\cdot i2ak'} \dots + e^{2\cdot i(N-1)ak'}\right] \tag{15}$$

$$\frac{e^{ibk'}-1}{ik'} \cdot \frac{1-e^{2\cdot iNak'}}{1-e^{2\cdot iak'}} = be^{i\frac{bk'}{2}} e^{i(N-1)\frac{ak'}{2}} \left(\frac{\sin\frac{bk'}{2}}{\frac{bk'}{2}}\right)\left(\frac{\sin Nak'}{\sin ak'}\right) \tag{16}$$

.

Thus, the intensity can be calculated by taking its square (eq17). Since in the experiment, the value of b is small enough, then with a small-angle approximation, it can be eliminated. As a result, by solving the equation, the light intensity is then calculated as in equation 17. Equation (eq17) shows that the intensity's maximum occurs at λ=2acosαcosβ/m, which is consistent with the discussion in the section 'Wavelength model', regarding the wavelength and light path differences. The intensity calculated from equation 17 also needs consideration of the spectrum of the filament lamp. Therefore, a ratio is added in front of the equation to represent the relative intensity of the filament light bulb at that specific wavelength, shown in Appendix A.

$$I = I_0 \left(\frac{\sin Nak'}{\sin ak'} \right)^2 = I_0 \left(\frac{\sin Na \frac{2\pi}{\lambda} \cos\alpha \cos\beta}{\sin a \frac{2\pi}{\lambda} \cos\alpha \cos\beta} \right)^2 \tag{17}$$

In the experiment comparison, the intensity of blackbody radiation at different wavelengths was considered using equation (eq18), where the temperature T was set at 3000 K. The constants k, h, and c represent the Boltzmann constant, the Planck constant, and the velocity of light respectively.

$$B(\lambda, T) = \frac{2hc^2}{\lambda^5} \frac{1}{e^{\frac{hc}{\lambda kT}} - 1} \tag{18}$$

(a) (b)

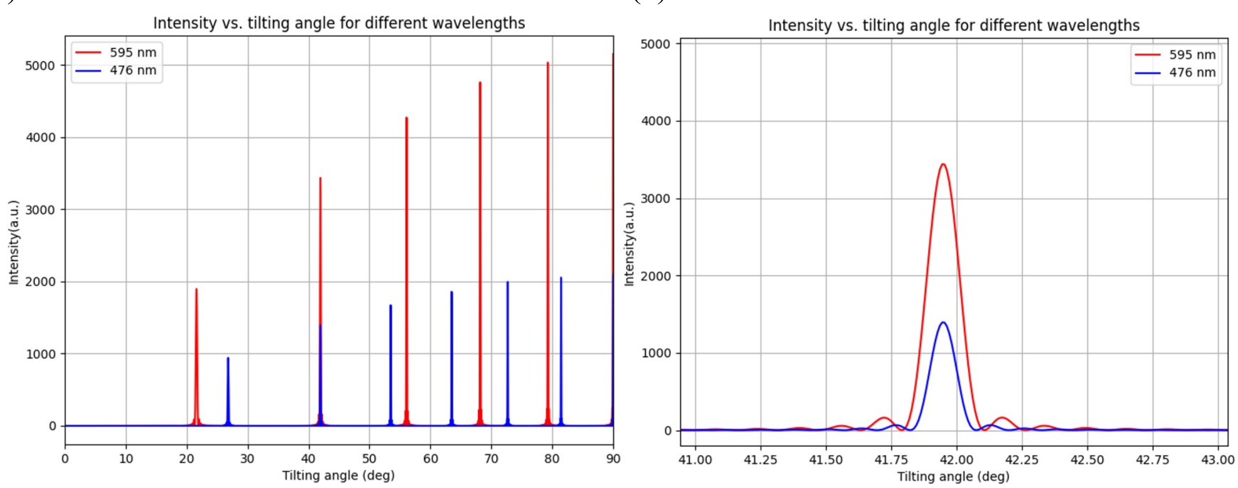

Figure 9. Numerical simulation of light intensity. (a) Light spectrum of 595 nm and 476 nm in different tilting angles (b) Close-up view of tilting angle approximately between 41 and 43 degrees, showing the wavelength superposition of two wavelengths at the tilting angle of 41.93 degrees.

Line equation in the general case

This section presents the calculation of the equation of the line corresponding to the tracks on the CD and their related properties, given the coordinates of the light source and the observer. The coordinate system's origin, A (0,0,0), is set at the center of the CD, with the z-axis perpendicular to the x-y plane. On the other hand, the plane of the CD, which is the x′−y plane, is derived using the concept of a family of planes as

$$E_{disc}: x - (\tan \alpha)z = 0 \tag{19}$$

The following model considers a point light source located at S(xs, ys, zs) and an observer at O(xo, yo, zo). Fu7rthermore, the tracks on the CD, which lie along the diameter, satisfy equal spacing and the conditions of the angles of incidence and reflection. Therefore, projecting vectors AS, and AO onto the x' — y plane and finding a plane where any point K on it ensures that the angles between vectors SK, and KO are equal and satisfy reflective diffraction. Thus, it yields the normal vector (eq20),

$$\vec{n} = (x_s d_o - x_o d_s, y_s d_o - y_o d_s, 0) \tag{20}$$

Where do, ds are the distances from the observer and the light source, respectively, to a point P(x,y,z) on the track. These distances can be defined as,

$$d_o = \sqrt{(x_o - x)^2 + (y_o - y)^2 + (z_o - z)^2}, d_s = \sqrt{(x_s - x)^2 + (y_s - y)^2 + (z_s - z)^2} \tag{21}$$

Since this plane passes through the origin, the equation of the plane (eq22) can be derived. The equation of the line representing the tracks on the CD is the intersection of two planes (eq23).

$$E_{bisect}: (x_s d_o - x_o d_s)x + (y_s d_o - y_o d_s)y = 0 \tag{22}$$

$$\begin{cases} x - (\tan \alpha)z = 0 \\ (x_s d_o - x_o d_s)x + (y_s d_o - y_o d_s)y = 0 \end{cases} \tag{23}$$

Thus, the line equation on the disc with a single light source is then calculated as,

$$\begin{cases} x = (\tan \alpha)t \\ y = \dfrac{t}{(y_s d_o - y_o d_s)} [\tan \alpha \, (x_o d_s - x_s d_o)] \\ z = t \end{cases} \tag{24}$$

Considering the geometric constraints of the CD track distribution, with a hollow part in the middle of the disc, the parameter t is thus constrained by,

$$0.046 \leq \sqrt{x^2 + y^2 + z^2} \leq 0.116 \tag{25}$$

Where 0.046m and 0.116m are respectively the radius of the inner hollow part and the overall size of a disc. Generalizing the wavelength and light intensity, the above methods of calculating the wavelength and light intensity can be applied to any light source and observer in space. The relevant angles can be expressed in coordinate form.

Based on Equation (eq24), numerical simulation yielded the line equation on the CD when the light source and observer were placed at points in space. In Figure 10, the light source was positioned at S (-1.5, 0.3, 0), and the observer was located at O (-1.5, 1, 0). The results indicate that the lines on the CD slightly incline towards the positive y-axis. The experimental verification of this inclination is presented in Appendix B.

$$\beta = \frac{1}{2}\cos^{-1}\left(\frac{(x_o - x)^2 + (y_o - y)^2 + [(x_s - x)^2 + (y_s - y)^2] - [(x_s - x_o)^2 + (y_s - y_o)^2]}{2\sqrt{(x_s - x)^2 + (y_s - y)^2}\sqrt{(x_s - x)^2 + (y_s - y)^2}}\right) \tag{26}$$

$$\delta = \cos^{-1}\left(\frac{\sqrt{(x_o - x)^2 + (y_o - y)^2}}{\sqrt{(x_o - x)^2 + (y_o - y)^2 + (z_o - z)^2}}\right) \tag{27}$$

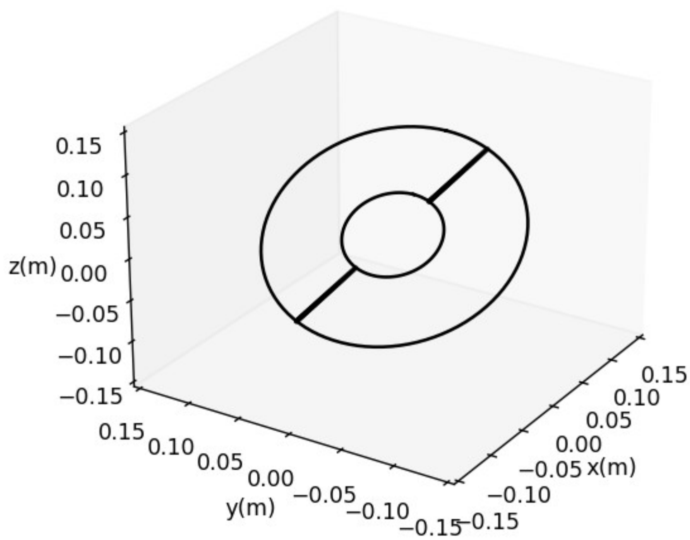

Figure 10. Numerical simulation of the line equation (24) on the disc – Results of the simulation, with the observer's position at O (-1.5, 1, 0) and the light source position at S (-1.5, 0.3, 0).

Cross-track interference experimental verification

To confirm cross-track interference, a laser with a specific wavelength was directed at the center of the disc. This experiment aimed to verify the presence of interfering light crossing between two tracks, in addition to observing diffraction orders for n=1. In the subsequent demonstration, a laser with a wavelength of 532 nm was used. As shown in Figure 11(b), the appearance of an additional diffraction line upon laser illumination supports the validity of the multiple-wavelength composition model in cross-track interference. This suggests the existence of multiple diffraction lines corresponding to higher n values, albeit with lower intensities. Consequently, these lines are difficult to detect with the naked eye or conventional cameras, yet their presence is confirmed.

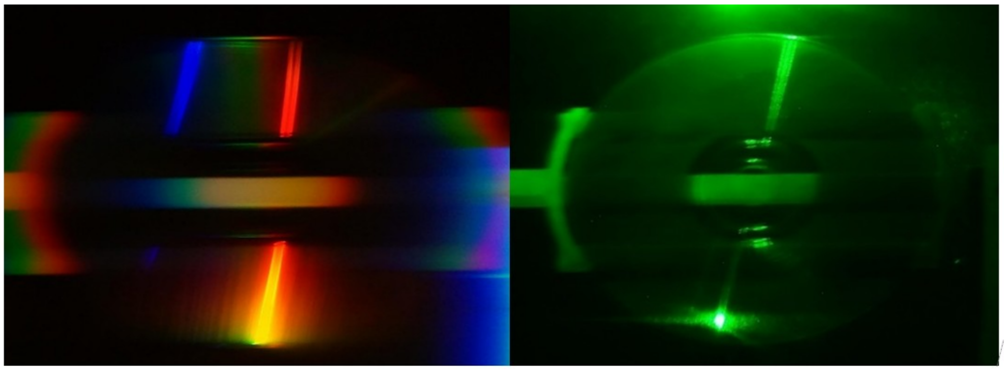

Figure 11. Experiment verification of cross-track interference with α=56°. (a) A blue and red diffraction line was found on the disc, with a faint green line appearing between them. (b) When illuminated with a 532 nm laser, a green diffraction line was observed, crossing two tracks. Although its intensity was lower, the line remained detectable.

Therefore, cross-track interference exists, and the constant n added in the model is necessary as shown in the equations below (eq28, eq29). The results of the numerical simulation further support this conclusion, demonstrating the appearance of an additional wavelength, as shown in Figure 12.

$$\lambda_m = \frac{n \cdot 2a \cos\alpha \cos\beta}{m} \tag{28}$$

$$I = I_0 \left(\frac{\sin Nak'}{\sin ak'} \right)^2 = I_0 \left(\frac{\sin n \cdot Na \frac{2\pi}{\lambda} \cos\alpha \cos\beta}{\sin n \cdot a \frac{2\pi}{\lambda} \cos\alpha \cos\beta} \right)^2 \tag{29}$$

As shown in Figure 12, it can be concluded that "Cross-track interference" generates two sets of wavelength data: one overlaps with "adjacent track interference," and the other corresponds to additional wavelengths. For example, at n=2, another peak appears at 510 nm, confirming the existence of cross-track interference and verifying the feasibility of this model. Taking α=56° as an example, the wavelengths of adjacent track diffraction (n=1) are 448 nm and 598 nm. Considering cross-track interference, a new wavelength of 510 nm appears at the same tilting angle, corresponding to the green lines under laser illumination in Figure 11(b). As the number of tracks between the interfering waves increases, lines of different wavelengths exist on the CD, yet with lower light intensity.

(a) (b)

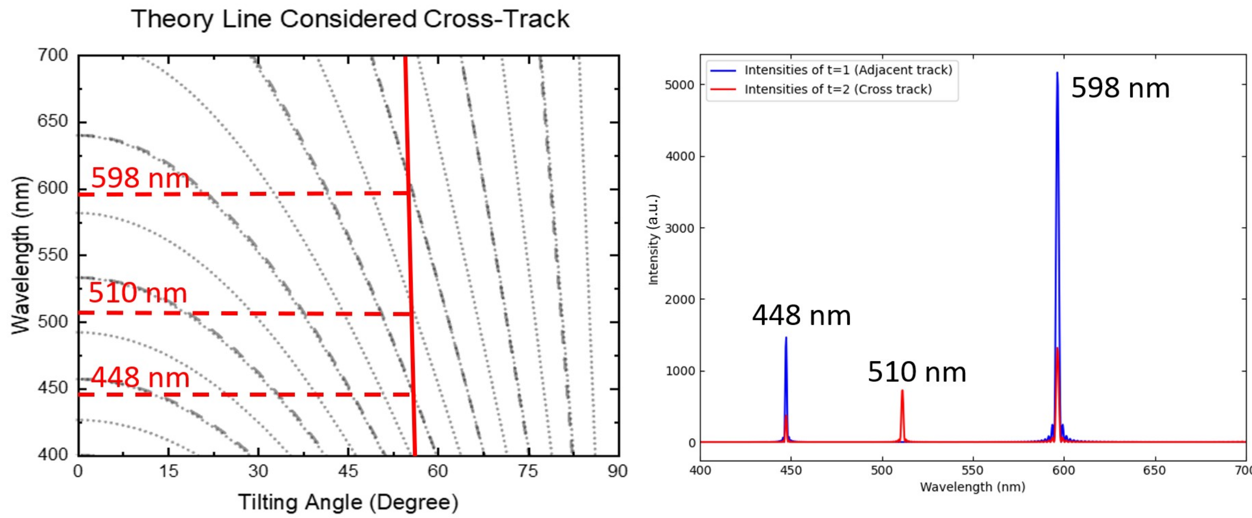

Figure 12. Numerical simulation of light wavelength and intensity. (a) Variation of light wavelength with tilt angle, considering theoretical lines for n=1 (dashed) and n=2 (dotted). (b) Spectrum of light when the CD is tilted at α=56° for n=1 (adjacent tracks) and n=2 (cross-track interference).

The experimental analysis is structured to systematically analyze diffraction effects on optical discs. Experiment 1 establishes the effect of tilting on wavelength and intensity, forming the basis for later studies. Experiment 2 examines wavelength distribution across the disc, while Experiment 3 explores different track spacing using CDs, DVDs, and BDs. Experiment 4 investigates how data recording alters diffraction patterns, and Experiment 5 explains line bending under close-range illumination. This sequence of experiments ensures logical progression, and validates the theoretical model.

Experiment 1: Influence of the tilting angle

An automatic rotating device and laser calibration were used to analyze how tilting angles affect wavelength and intensity. All experiments in this section used unrecorded CDs with β=0. Experiments with and without a prism were compared.

First, experiments without a prism showed a clear line in the middle of the disc. As the tilting angle increased, the wavelength showed a negative correlation. When a prism was introduced, the reflected light was dispersed into monochromatic light, allowing comparison with the theoretical predictions shown in Figure 14(b). Overall, the experiments matched the trend, with an average deviation of 3.2% and a relative standard deviation of 1.6%. However, at 30 degrees in the fourth diffraction order, the experimental wavelength was noticeably lower than the theoretical value by approximately 30 nm. This discrepancy was due to the lower intensity of the filament lamp as it approached the IR region, making the line less visible and its position harder to determine.

When investigating intensity, diffraction order and tilting angle were positively correlated due to the filament lamp's spectrum, demonstrated in Appendix A, and the increasing illuminated area. It was noted that the intensity was significantly lower at 30 degrees, as the smaller illuminated area and light reflection between tracks led to energy absorption and a reduction in intensity.

(a) (b)

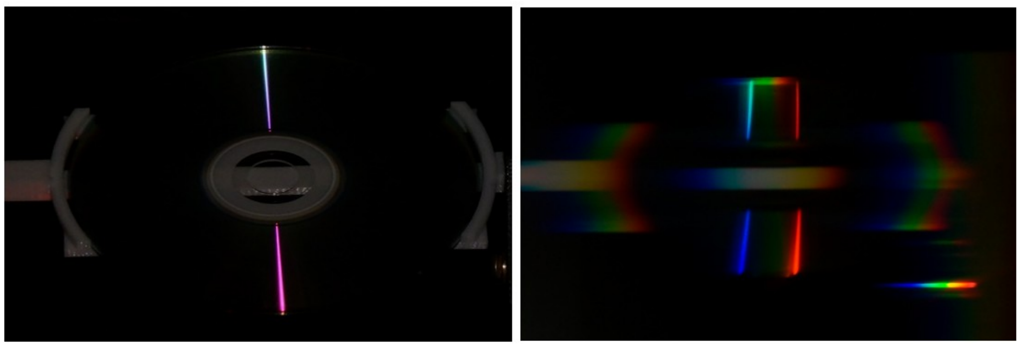

Figure 13. Experiment demonstration of the lines observed. (a) Without a prism, a single diffraction line is observed. (b) With a prism, multiple lines of different wavelengths appear on the disc.

(a) (b)

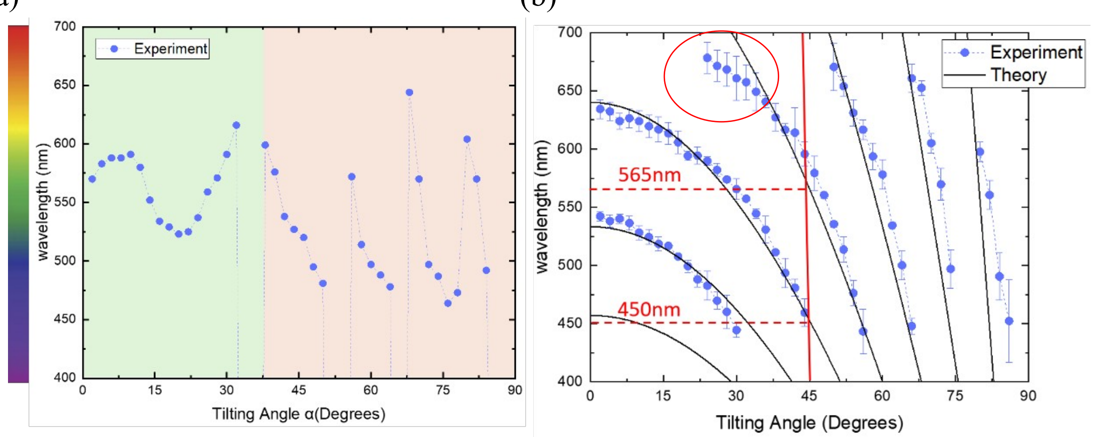

Figure 14. Experiment results and theoretical predictions regarding wavelength for Experiment. (a) In experiments without a prism, the wavelength fluctuates between 525 to 625 nm under a small angle, because of the wavelength superposition. With a bigger angle, a negative correlation is observed. (b) In experiments with a prism, both theory and experiments agree that wavelength is negatively correlated. Besides, the superposition of wavelength can be observed. Taking 45 degrees as an example, the resulting wavelength is a combination of 565 and 450 nm.

(a) (b)

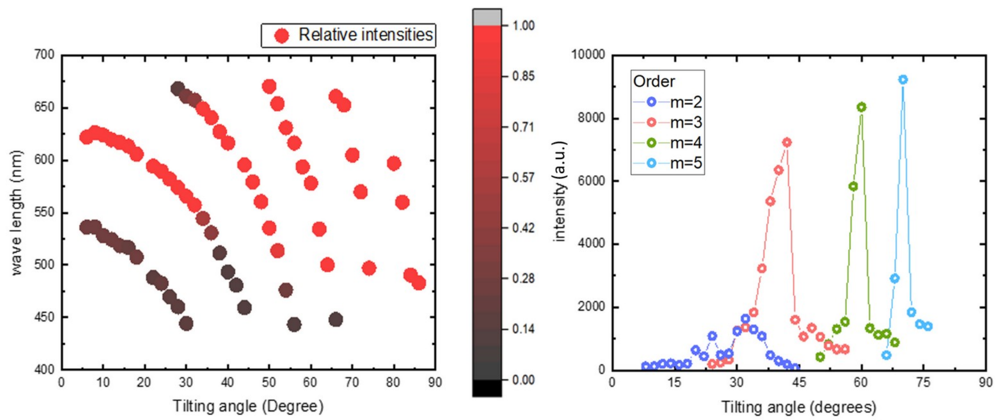

Figure 15. Experimental results and theoretical predictions regarding intensity for Experiment 1. (a) Relative intensity in different tilting angles. The stronger wavelength under a particular angle is set as one and normalized to the others. (b) Absolute intensity at different tilting angles and different orders. The first order was often out of focus because of the large inclination of the line, and the sixth and seventh orders were too complex to be investigated due to their low intensities.

Experiment 2: wavelength distribution on the disc

When light is diffracted by the disc, different positions on the disc affect the incident angle of the light, causing differences in wavelength and intensity. With a larger effective tilting angle, the wavelength at the bottom part of the disc decreased. The wavelength increased linearly within a small range as it reached the top part of the disc.

(a) (b)

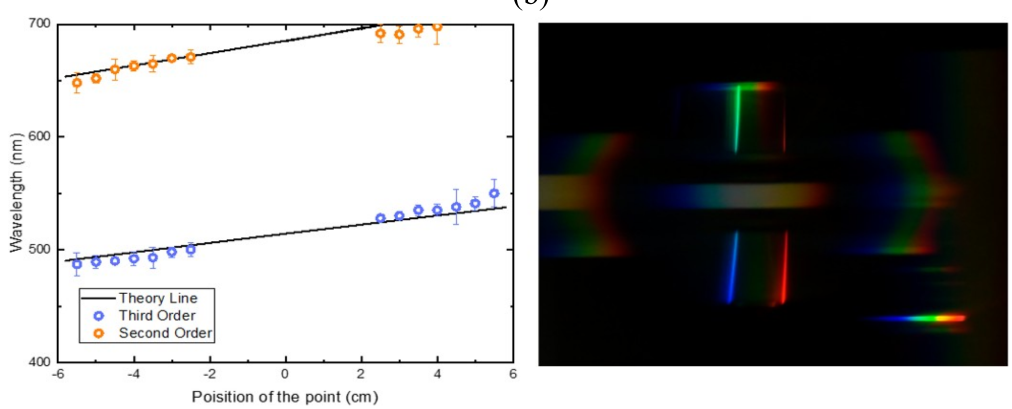

Figure 16. Experimental results data and theoretical prediction for Experiment 2 — Wavelength distribution. (a) Comparison of wavelength distribution with α=48°. The blue and orange dots are the experimental data of the third and the second diffraction order, respectively. (b) Experimental figure of the line shown from the grating with a 48 degree tilting angle.

Under these experimental conditions, with α=48°, both theoretical predictions and experimental results demonstrated that the wavelength of the third diffraction order exceeded the upper bound of the visible spectrum, entering the infrared (IR) region. This phenomenon is shown in Figure 16(b), where the diffraction line in the upper area is not visible.

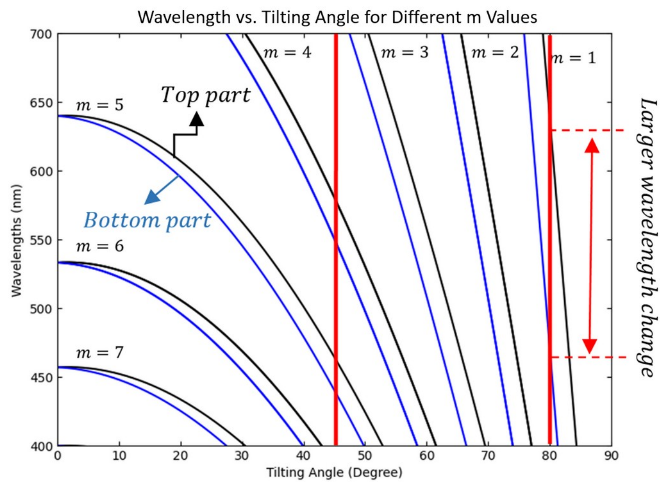

Figure 17. Wavelength changes with tilting angles with different m values. Theoretical curve considering the light distribution for Experiment 2, where the blue solid line represents the bottom boundary of the wavelength, and the black curve indicates the upper bound.

Experiment 3: different pitches (CD/DVD/BD)

The use of DVDs or BDs (Blu-ray Discs) for light reflection significantly affected the results due to the different values of a, representing the distance between adjacent tracks. Unlike compact discs with a pitch of 1608 nm, DVDs have a smaller pitch of 740 nm, and BDs have an even smaller pitch of 320 nm. As illustrated in Figure 18, a smaller track distance resulted in fewer theoretical curves. As predicted in Figure 19, this reduction compressed the theoretical diffraction curves of the CD vertically. The experimental observations found only a single curve for BDs, as shown in Figure 18(b).

The range of tilt angles at which lines on BD discs are visible within the visible light spectrum was smaller compared to DVDs and CDs. This occurred due to the narrower pitch and lower diffraction orders, restricting the range of tilting angles where lines were observable on the disc. As shown in Figure 19, at smaller tilt angles and larger track spacings, composite light overlaps were more pronounced. With the track width of a BD, the range of existing wavelengths was smaller and there was less overlap. In contrast, CDs showed more noticeable wavelength superposition.

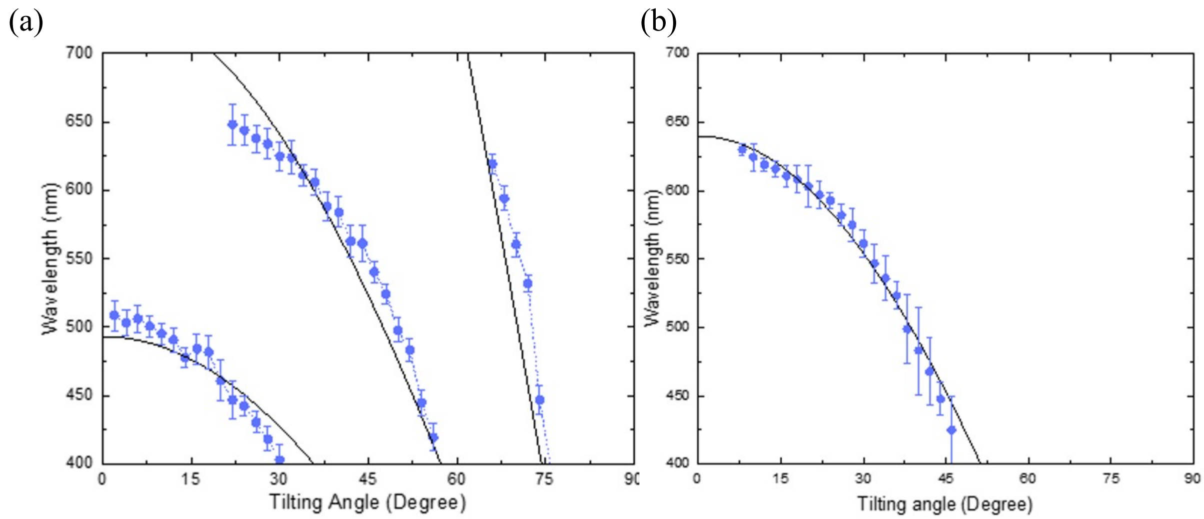

Figure 18. Experimental data and theoretical predictions of Experiment 3. Experiment data of different pitches (a) DVD with 740 nm and (b) Blue-ray disc with 320 nm are shown. Blue dots represent experimental data, and the solid black line is the theoretical prediction.

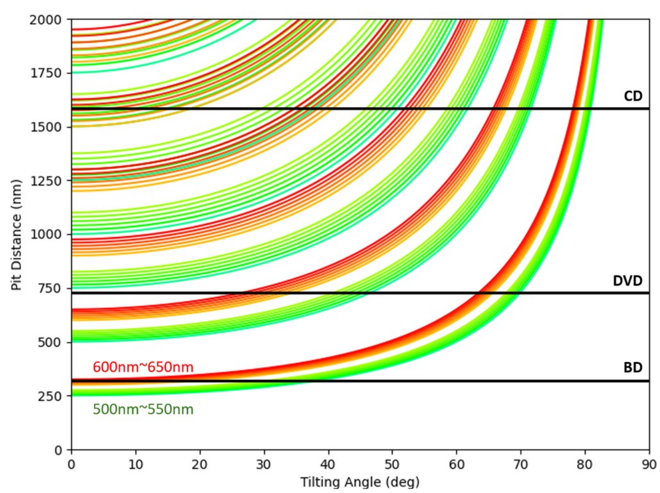

Figure 19. Theoretical prediction of the influence of the pitch and the tilting angle of Experiment 3. The green lines represent wavelengths ranging from 500 to 550 nm from bottom to top, while the red lines have wavelengths ranging from 650 to 660 nm. Besides, three horizontal lines with the graph are the pitches of CD, DVD, and BD, from top to bottom.

Experiment 4: Influence of the recording of CD

During the recording process, the disc's tracks are carved to store information, making the back of the disc a non-continuous structure. In the experiments, a CD burner was used to record single-tone audio files with varying sizes: 150 MB, 300 MB, and 500 MB. These files were generated using Audacity 3.4 (Audacity), with 1 kHz tones to allow for comparison of diffraction patterns.

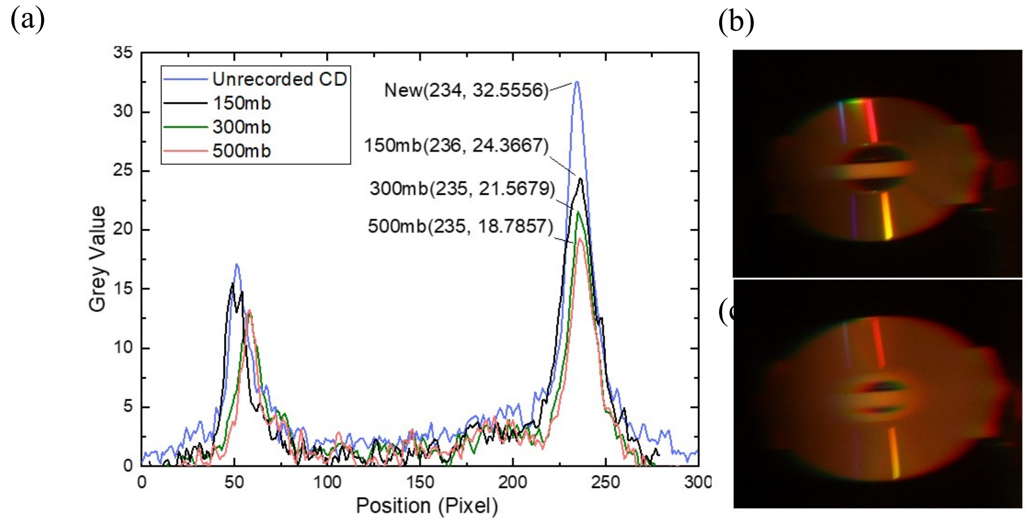

Figure 20. Experimental data and theoretical predictions of Experiment 4. (a) Relative light intensity data at different positions on the disc with a tilting angle of 50°. An unrecorded disc, and recording with 150 MB, 300 MB, and 500 MB files are shown in the figure in blue, black, green, and red lines. Grey values represent the brightness level of a pixel, ranging from 0 to 255, and were obtained using ImageJ. (b) Experimental photo of an unrecorded disc at the same tilting angle. (c) Experimental photo of a recorded disc with 500 MB at the same tilting angle.

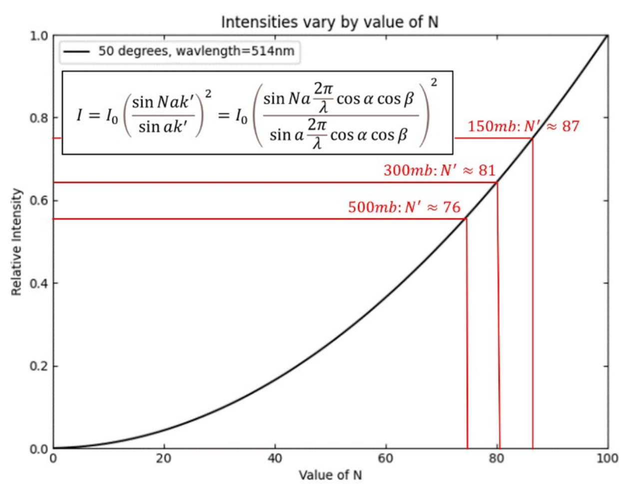

Figure 21. Variation of relative light intensity with the number of tracks. The relative light intensity measurements enabled the estimation of the effective number of tracks in the discontinuous structures. The red line indicates the corresponding number of tracks with different file sizes recorded on the CD. The black solid curve represents the theoretical prediction derived from the equation shown in the figure.

After recording, the dye layer on the back of the disc was burned, creating a reflective rate difference. Since this effect occurred uniformly across all light frequencies and cross-track interference was considered, the recording process did not affect the wavelength. However, it significantly affected the intensity of the light, as shown in Figure 20(a). With a larger file recorded, more tracks at the back of the disc were burned, thus decreasing the intensity of the light, as seen in Figures 20(b) and 20(c).

Since the recorded disc's tracks form a non-continuous structure, determining the value of N was challenging, even with microscopic analysis. However, the effective number of tracks could be estimated using the intensity ratio compared to the unrecorded disc, as shown in Figure 21. Analysis revealed that the effective number of tracks for recorded discs of 150 MB, 300 MB, and 500 MB was 87, 81, and 76, respectively.

Experiment 5: The bending of the line

In the original experimental setup, the lines on the disc appeared linear and unbent. However, when the disc was illuminated from a short distance, line bending occurred, as shown in Figure 22, where the light was placed at (-0.02,0.15,0.08), 8.3 cm from the center of the disc.

For analyzing the lines on the disc, equal spacing between slits along the diameter and meeting the far-field definition remain essential considerations. The experimental observations suggested that the angle difference of the point light source at different positions on the disc caused the lines to bend at close range. Through multiple trials, bending lines consistently appeared when the light source and observer were near the disc. After applying the parametric equation (eq30) to simulate this close-range effect in Figure 22(b), the model successfully described the observed line bending, as shown in Figure 23.

$$\begin{cases} x = (\tan\alpha)t \\ y = \dfrac{t}{(y_s d_o - y_o d_l)}[\tan\alpha\,(x_o d_l - x_s d_o)] \\ z = t \end{cases} \tag{30}$$

$$d_o = \sqrt{(x_o - x)^2 + (y_o - y)^2 + (z_o - z)^2}\; d_s = \sqrt{(x_s - x)^2 + (y_s - y)^2 + (z_s - z)^2} \tag{31}$$

In this context, do and ds function as parameters of (x,y,z). Initially, due to the distance between the light source, observer, and disc, these parameters remained approximately constant while the disc position changed. However, when the light source and observer coordinates were positioned close to the disc, the straight line transformed into a curve intersecting with the disc, as demonstrated in Figure 22(b). The numerical simulation of the line conducted using equation (eq30) is presented in Figure 23. The substantial degree of line bending observed likely resulted from a non-parallel light incident on the back of the disc at a small distance. This incident angle caused the reflection from the uneven surface and the protective layer of the disc to affect the light path, leading to observable deviations.

(a) (b)

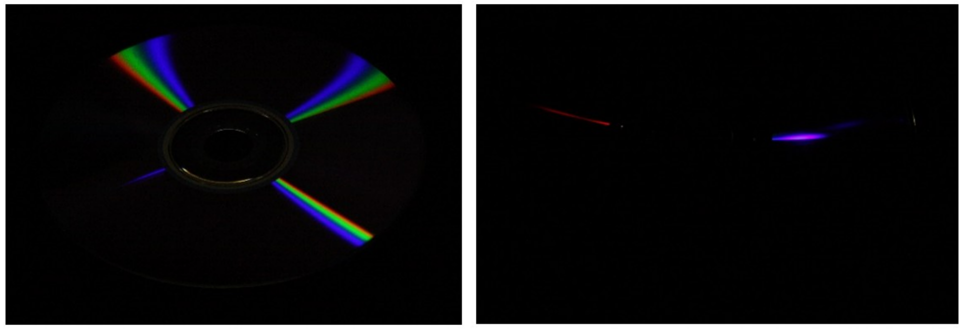

Figure 22. Experimental observation of the bending of the diffraction line. (a) The bending of lines under multiple light sources. (b) The bending of a line under a single light source.

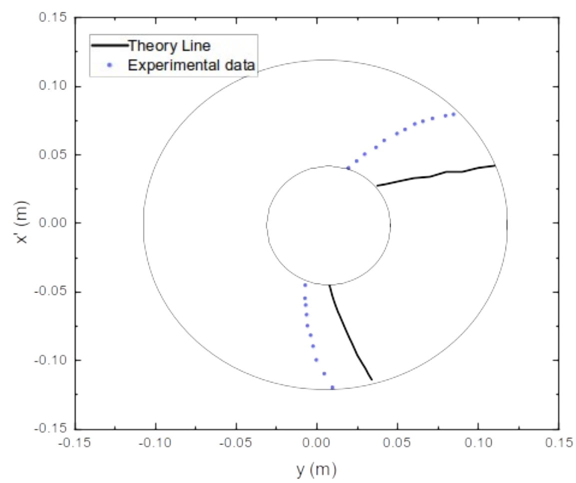

Figure 23. The simulation and experimental comparison of the bending line in Experiment 5, where the light source at S (-0.02, 0.015, 0.08) and the observer at O (0.01, -0.1, 0.015).

Practical applications

The optical characteristics of a CD, specifically the diffraction pattern produced by the spacing of tracks, offer a unique way to analyze light sources. This research developed a device capable of measuring the angles of incident light. When illuminated at different angles, the tracks on the CD produced diffracted lines that were visible to a smartphone camera. The positions of these lines demonstrated high sensitivity to the angle at which the light struck the disc.

The experimental setup involved vertical observation of the upper half of the CD using a smartphone camera equipped with a prism. Then, the image was transferred to a computer, where OpenCV 4.5.5 (Open-Source Computer Vision Library) was employed to analyze the lines. Following the line position and wavelength mapping, the analysis utilized Appendix B and equation (eq28) to determine the angle of incident light.

This developed methodology provides a practical approach for analyzing incident light direction. Such measurements have potential applications in fields requiring precise characterization of light angles and wavelengths, offering a straightforward method for optical analysis.

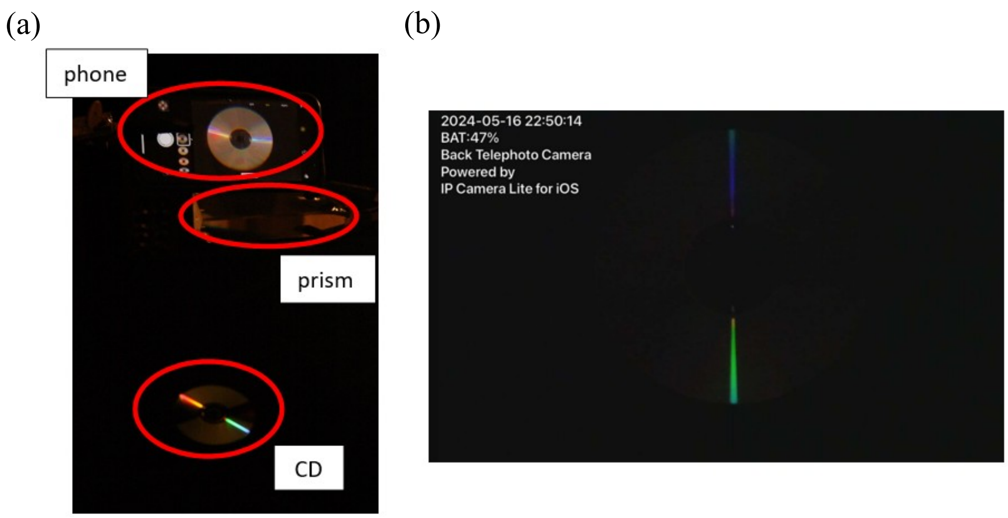

Figure 24. (a) Experimental photograph of the light source sensing device. (b) An analytical photograph, captured by linking the mobile phone camera using OpenCV technology.

Conclusion

The wavelength, intensity, and the equation of the line observed on a disc with a single light source were modeled. The concentric tracks on the back of a CD acted as a reflective diffraction grating in this case. Thus, the optical path difference created by light waves incident on tracks resulted in the formation of colored lines on the disc. Laser calibration and prism dispersion enabled mapping specific wavelengths to CD positions for wavelength analysis. The tilting angle α exhibited a negative correlation with the wavelength for the same diffraction order m. Due to the viewing angle difference, the wavelength distribution varied across different positions, with longer wavelengths observed at the upper end of the disc. The track pitch of the disc was positively correlated with the wavelength, leading to more color variations and wavelength overlaps in the visible range for CDs compared to DVDs and CDs. Cross-track interference was confirmed, producing lines on the disc with lower light intensity. The light intensity was negatively correlated with the number of tracks crossed. CD burning significantly reduced diffraction efficiency, and the light intensity was found to be proportional to the square of the number of tracks based on the different file sizes burned. Utilizing the properties of diffraction gratings, it was possible to successfully simulate the position, wavelength, and light intensity of the lines on the CD given any observer and light source coordinates in space. When the light source and the observer were positioned close to the disc, under point source conditions, the line on the disc transitioned from a straight line into a curve.

Acknowledgments

I would like to acknowledge my physics teacher Mr. Kou for helping me research this phenomenon, discussing experimental data with insights. In addition, I would also like to thank sophomore Hsin-Yuan Lin from the National Central University for providing valuable comments on the experimental apparatus.

Abbreviations

a: Pitch of a disc, which is the distance between adjacent tracks (nm), α: Tilting angle of the disc (deg), β: Rotating angle (deg), θ: Viewing angle (deg), m: diffraction order, λ: Wavelength (nm), I: Light intensity, d: Distance from the camera to the observer (m), k: Wave number, N: number of tracks on the disc, n: Cross-track interference constant, r: Radius of the disc (m), R: Radius of the central, hollow part of the disc (m).

References

1. Ngamaroonchote, A., Chotsuwan, C., Tantisantisom, K., Laocharoensuk, R. (2017). Patterned gold electrode prepared from optical discs display largely enhanced electrochemical sensitivity as exemplified in a sensor for hydrogen peroxide. *Microchimica Acta*, 184(1), https://doi.org/10.1007/s00604-016-2008-z

2. Noldeke, C. (1990). Compact disc diffraction. *The Physics Teacher,* 28(8), 484–485. https://doi.org/10.1119/1.2343118

3. Balachandran, R., Porter-Davis, K. (2020). CDs and DVDs as diffraction gratings. *NNCI Nano* https://nanohub.org/resources/31937

4. Haym, K. (1993). Diffraction demonstration with a compact disc. *The Physics Teacher,* 31(2), 104. https://doi.org/10.1119/1.2343673

5. Cope, J. A. (1993). The physics of the compact disc. *Physics Education,* 28(1), 15–21. https://doi.org/10.1088/0031-9120/28/1/003

6. Cai, B., Mainhood, L., Groome, A., Laverty, C., Moffat, A. (2021). Student behavior in undergraduate physics laboratories: Designing experiments. *Physical Review Physics Education Research,* 17(2), 020109. https://doi.org/10.1103/PhysRevPhysEducRes.17.020109

7. Fernandez-Dorado, J., Hernandez-Andrez, J., Valero, E. M., Nieves, J. L., Romero, J. (2008). A

simple experiment to distinguish between replicated and duplicated compact discs using Fraunhofer diffraction. *American Journal of Physics,* 76(12), 1137–1140. https://doi.org/10.1119/1.2980581

8. DeLuca, R., DiMauro, M., Fiore, O., Naddeo, A. (2018). A compact disc under skimming light rays. *American Journal of Physics,* 86, 169-173.. https://doi.org/10.1119/1.5021904

9. Fowles, G. R. (1989). Introduction to Modern Optics (2nd ed.), Chapter 5.4 Fraunhofer Diffraction Patterns. Dover Publications, New York, USA.

10. Serway, R. A., Jewett, J. W. (2009). Physics for Scientists and Engineers with Modern Physics (8th ed.). Cengage Learning, Boston, MA, USA, p. 1122.

Appendix A. Spectrum for filament lamp used in the experiment

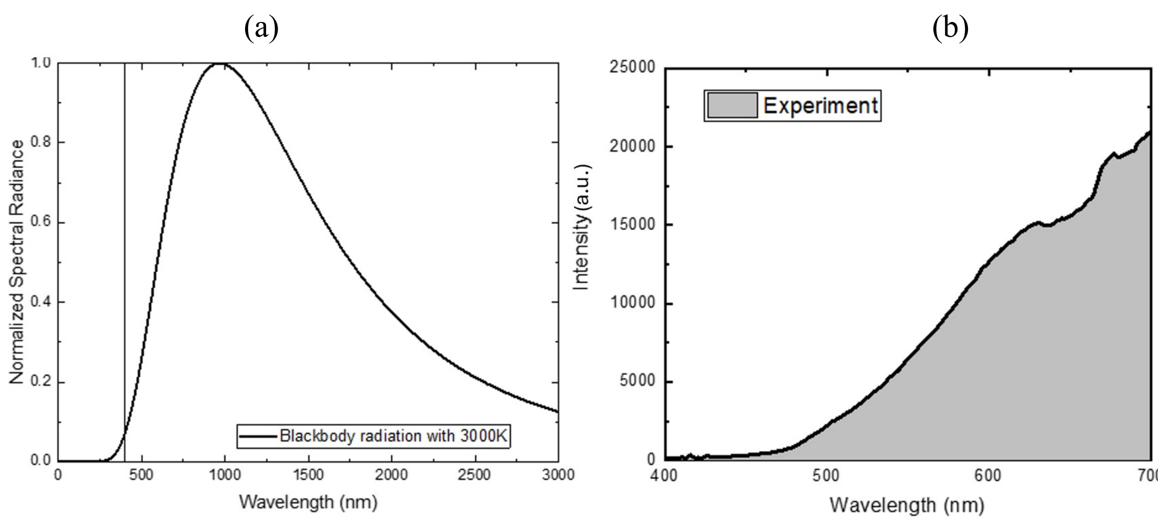

Figure 25. Spectrum for filament lamp (a) Blackbody radiation with temperature as 3000K (b) The light spectrum of the filament lamp used in the experiment.

Appendix B. Inclination of the line

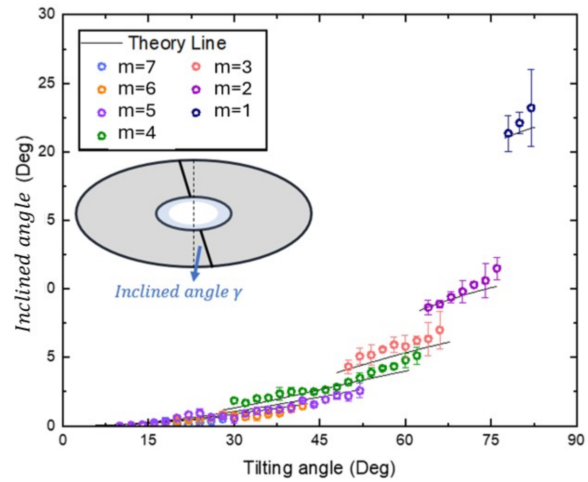

Figure 26. Comparison of theory and experiment data related to the inclination of the line with different tilting angles.

$$\gamma = \sin^{-1}\left[\frac{(\lambda_{top} - \lambda_{bottom}) \times \delta}{2r}\right] = \sin^{-1}\left[\frac{4a\cos\beta\sin\alpha\sin\theta_{max} \times \delta}{rm}\right] \tag{32}$$

Where θ_{max} is the maximum viewing angle, to show the wavelength gradient and δ represents the number of pixels changed per wavelength change.